Quaternary Science Reviews 164 (2017) 25–36

Contents lists available at ScienceDirect

Quaternary Science Reviews

journal homepage: www.elsevier.com/locate/quascirev

Hemispherically in-phase precipitation variability over the last 1700 years in a Madagascar speleothem record

Nick Scroxton [a, *], Stephen J. Burns [a], David McGee [b], Ben Hardt [b], Laurie R. Godfrey [c], Lovasoa Ranivoharimanana [d], Peterson Faina [d]

[a] Department of Geosciences, 611 North Pleasant Street, University of Massachusetts, Amherst, MA 01003, USA
[b] Department of Earth, Atmospheric and Planetary Sciences, Massachusetts Institute of Technology, 77 Massachusetts Avenue, Cambridge, MA 02139, USA
[c] Department of Anthropology, 240 Hicks Way, University of Massachusetts, Amherst, MA 01003, USA
[d] Mention Bassins Sédimentaires, Evolution, Conservation (BEC), BP 906, Faculté des Sciences, Université d'Antananarivo, 101 Antananarivo, Madagascar

ARTICLE INFO

Article history:
Received 9 December 2016
Received in revised form
17 March 2017
Accepted 18 March 2017
Available online 30 March 2017

Keywords:
Holocene
Paleoclimatology
Monsoon
ITCZ
Madagascar
Southern hemisphere
Speleothems
Stable isotopes
U-Th series

ABSTRACT

Paleoclimate studies of tropical rainfall have led to a recognition of a predominant pattern of anti-phase behavior between the Northern and Southern hemispheres at both orbital and millennial timescales. Less certain is how regional tropical rainfall patterns have changed in the late Holocene, under boundary conditions and on timescales which are most relevant to the tropics' response to a warming world. Several high-resolution southern hemisphere rainfall records are at odds with meridional movement of the mean Inter-Tropical Convergence Zone location as the major driver of Holocene tropical rainfall variability, with regional precipitation patterns resembling modern day El-Niño Southern Oscillation end members. To test emerging ideas on sub-millennial tropical rainfall variability, additional records from the southern hemisphere are required.

We present a new speleothem $\delta^{18}O$ record from Anjohibe Cave, northwestern Madagascar, which provides a quasi-annual record of monsoonal strength and precipitation amount for the last 1700 years. The majority of $\delta^{18}O$ variability in the record is at the decadal scale, and shows little to no correlation with major climate indices or cyclical climate drivers. At lower frequencies, changes in mean speleothem $\delta^{18}O$ show good correlation with other regional precipitation records both north and south of the equator. The regional coherency of tropical rainfall across the west Indian Ocean resembles expansion and contraction of the tropical rain belt and positive-Indian Ocean Dipole-like conditions at different timescales. The cause of this coherency could be related to symmetrical changes in continental sensible heating, or to a low frequency sea surface temperature climate mode.

1. Introduction

Year to year variation in rainfall has a dramatic impact on the health and prosperity of people in the tropics, particularly in socioeconomically vulnerable regions such as eastern Africa (Hashizume et al., 2009). Despite some recent improvements, Madagascar is one of the ten poorest countries in the world, with a per capita GDP of $443 (World Bank, 2015), 70% of the population living in poverty and the fourth lowest access to water in Africa (UNICEF, 2012). Four out of five people are dependent on rain fed agriculture (Macron et al., 2016). Madagascar is particularly vulnerable to hydrological natural disasters with frequent tropical cyclones, droughts and flooding. One quarter of the population resides in zones rated at risk of natural disasters (GFDRR, 2013). Understanding of hydrological variability in Madagascar is therefore critical to the lives and wellbeing of millions in this understudied region. Yet instrumental records of rainfall in Madagascar are short and frequently discontinuous, hindering understanding of what factors influence rainfall variability on interannual and longer timescales.

The seasonal and spatial distribution of Madagascan rainfall is largely controlled by two factors: the central massif along eastern Madagascar, which consists of a broad 1200 m high plateau with peaks up to 2876 m, and the annual migration of the ITCZ. During austral winter the Mascarene high to the southeast of Madagascar brings onshore trade wind easterlies to the island (Fig. 1). The central massifs create orographic rainfall on the east coast and a

* Corresponding author.

http://dx.doi.org/10.1016/j.quascirev.2017.03.017
0277-3791/

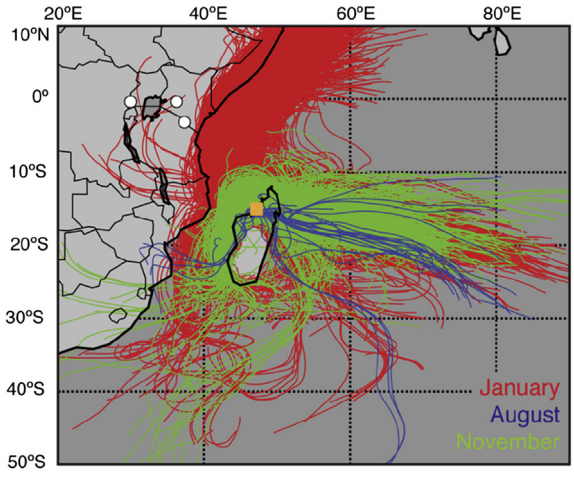

Fig. 1. Air parcel 120hr back trajectory simulations indicating likely moisture source areas for precipitation at Anjohibe (yellow rectangle). Trajectories shown for wet season (January, red), shoulder season (November, green) and dry season (August, blue). Trajectories were launched at 500, 1000 and 1500 m every 6 h for GDAS data between 2005 and 2015 using Python package PYSPLIT (Cross, 2015) on top of the NOAA HYSPLIT model (Stein et al., 2015). Only rain bearing trajectories and those with a forward integration error of less than 10% were used. White circles indicate other paleoprecipitation records discussed in the text. From west to east: Lake Edward, Lake Naivasha, Lake Challa.

rain shadow to the west that extends across the entire island. The result is a strong east to west rainfall gradient. During austral summer the Mascarene high weakens and retreats to the southeast whilst the ITCZ moves southwards into the Mozambique channel reaching 15°S (Jury and Pathack, 1991). Northwesterly winds bring monsoonal rains to most of the island and create a strong north to south rainfall gradient. Northwestern Madagascar is therefore insulated against trade-wind derived precipitation and exposed to variability in the monsoon.

Interannual variability of rainfall on Madagascar is not well constrained due to a paucity of lengthy instrumental records. Poor correlation between regional outgoing longwave radiation and Madagascan rainfall (Jury et al., 1993) suggests that local influences dominate Madagascan rainfall. As a consequence, studies using a combination of convection processes and zonal climate modes, such as the Southern Oscillation Index (SOI), Madden Julien Oscillation (Jury et al., 1995), and the Quasi-Biennial Oscillation (Macron et al., 2016), fail to explain much of Madagascan rainfall variability. Links between Madagascan rainfall and El-Niño-Southern Oscillation (ENSO) are typically made by correlation with regional rainfall rather than direct one-to-one association (Brook et al., 1999; Goddard and Graham, 1999).

A major driver of west Indian Ocean hydroclimate and sea surface temperature (SST) variability is the Indian Ocean Dipole (IOD). The IOD is an oscillatory zonal climate mode not dissimilar to ENSO, but largely restricted in its atmospheric influence to the boreal spring (coinciding with the short rains of equatorial East Africa). During positive phases of the IOD an increase in the average east to west SST gradient and wind strength brings wetter austral spring conditions to the equatorial west Indian Ocean (Saji et al., 1999; Webster et al., 1999). The IOD has good correlation and mechanistic links with ENSO, but IOD events can also result from internal Indian Ocean dynamics alone (Goddard and Graham, 1999), suggesting a degree of independence from ENSO (Ashok et al., 2003). IOD atmospheric anomalies are unlikely to influence west Madagsacan rainfall due to the orographic isolation that prevents trade-wind derived precipitation from reaching the western half of the island.

The IOD also influences regional sea surface temperatures, and there is strong evidence for an SST signal in regional precipitation in the west Indian Ocean region, both in the modern and the past in East Africa (Black et al., 2003; Hastenrath et al., 2004; Nakamura et al., 2011; Nash et al., 2016) and South Africa (Jury et al., 1995, 1993). A link between west Indian Ocean SSTs and Madagascan rainfall has also been hypothesized (Brook et al., 1999). However, instrumental records and ERA-interim climate reanalysis show no correlation between monthly SST anomalies and monthly rainfall in northwestern Madagascar, except in December ($r = 0.377$, $p = 0.021$). Due to the seasonal locking of the IOD the maximum interannual variability of SSTs in the west Indian Ocean is typically between September and November, before the Madagascan monsoon season between December and March (Schott and McCreary, 2001). While austral spring SST anomalies can influence austral summer rainfall (e.g. in the Seychelles (Harou et al., 2006)), this appears not to be the case further from the equator in Madagascar.

Lower frequency SST modes may circumvent the seasonal locking of the IOD and influence Madagascan rainfall. At decadal or longer timescales the mean state of the IOD is relatively unknown. Indian Ocean SST records of the last 100 years indicate significant decadal variability in the IOD (Abram et al., 2008; Ault et al., 2009; Nakamura et al., 2009), while millennial scale variations in the mean IOD state and seasonality are expected due to the evolution of the Asian monsoon intensity and ENSO variability through the Holocene (Abram et al., 2007). However, both the power of the IOD at the decadal scale (Ashok et al., 2003, 2004) and its relationship to regional precipitation (Konecky et al., 2014) is non-stationary. Thus, it remains to be determined whether changes in mean west Indian Ocean SST and/or IOD behavior may influence Madagascan rainfall on longer timescales.

In contrast to these zonal climate mechanisms, meridional changes in the monsoon may have a significant impact on interannual rainfall variability in Madagascar. The evidence for meridional ITCZ influences on southern hemisphere tropical rainfall at a variety of timescales is well founded. At millennial and orbital timescales precipitation in monsoonal regions has been shown to be modulated by changes in meridional circulation, typically due to movements in the Inter-Tropical Convergence Zone (ITCZ) (Haug et al., 2001; Liu et al., 2003; Schneider et al., 2014; Verschuren et al., 2009). Periods of higher summer insolation are associated with increased summer monsoon rainfall in both hemispheres, leading to anti-phase behavior of the Northern versus Southern Hemisphere monsoons on precessional timescales (X. Wang et al., 2006; Y. Wang et al., 2008). Similar anti-phased changes in rainfall are associated with rapid millennial-scale changes in temperature in the high northern latitudes during the last glacial period. During stadial events in the Greenland ice cores, the northern hemisphere monsoons weakened while the southern hemisphere monsoons intensified (Ayliffe et al., 2013; Denniston et al., 2013; Kanner et al., 2012; X. Wang et al., 2007).

At sub-millennial timescales, there is debate over whether the ITCZ translates north and south or whether it expands and contracts, widening and shrinking the width of the tropical rain belt. Over the late Holocene both anti-phase (Eroglu et al., 2016) and in-phase (Denniston et al., 2016) behavior have been described for the northern and southern hemisphere counterparts of the East Asian summer monsoons (EASM). Out of phase behavior suggests translation of the ITCZ north and south either due to a shift in the seasonal range or a change in the amount of time spent near one seasonal extreme. In-phase behavior implies a symmetrical expansion and contraction of the tropical rain belt. During the Little Ice Age (LIA) between the 16th and 18th centuries, it is expected that greater cooling of the northern hemisphere drives a more

southerly mean location of the ITCZ (Broccoli et al., 2006; Zhang and Delworth, 2005). Yet observations show that dry conditions occurred at both the northern and southern peripheries of the East Asian monsoons, with wetter conditions around the equator (Yan et al., 2015), describing a contraction of the tropical rain belt. This response may be specific to individual monsoon systems: wetter conditions are observed in the South American Summer Monsoon (SASM) domain during the LIA (Vuille et al., 2012). Thus, for centennial scale variations during the Holocene it is not entirely clear whether meridional or zonal changes in atmospheric circulation exert a stronger control on the monsoons for a particular region. Local and regional climatic idiosyncrasies appear to alter the sensitivity of individual monsoon systems to zonal feedbacks that arise from meridional forcings.

Together, meridional and zonal climate mechanisms likely interact to create a more complex pattern of precipitation patterns that cannot easily be explained by either forcing individually. During the LIA, east-west antiphasing of hydroclimate proxies across the Pacific set up a "La-Niña-like" rainfall pattern, indicating a major role of Pacific zonal Walker circulation in controlling tropical hydroclimate (M. L. Griffiths et al., 2016) during a southward ITCZ shift (Sachs et al., 2009). Around East Africa an "El-Niño-like" precipitation pattern occurred during the LIA (Russell and Johnson, 2007; Tierney et al., 2013). Lake Malawi in the African rift valley experienced windier but drier conditions - a weakening in the Congo Basin African Monsoon reduced moisture transport to the African rift valley south of the equator despite more southerly ITCZ circulation patterns (Brown and Johnson, 2005; Russell and Johnson, 2007; Vellinga and Wood, 2002). In the Horn of Africa, records from Lake Challa and Lake Naivasha and the Gulf of Aden show wet conditions during the Little Ice Age (Tierney et al., 2013, 2011; 2015; Verschuren et al., 2009, 2000). This equatorial Horn-Rift dichotomy during the Little Ice Age has been attributed to zonal Walker Cell dynamics controlled by the Indian Ocean (Tierney et al., 2013) but has also been related to meridional variability (Tierney et al., 2015).

There are climatic similarities between East Africa and Madagascar as they share a dominant moisture source: the equatorial west Indian Ocean. Therefore, oceanic changes will likely influence both areas. However, there are strong atmospheric differences between East Africa and Madagascar. East African records are difficult to interpret due to competing influences between the balance of Indian Ocean and Atlantic Ocean sourced moisture, and changes in the short versus long rains (Nash et al., 2016; Tierney et al., 2015). Northwestern Madagascar, with its single summer rainy season and single dominant water vapor source, provides a much simpler climatic setting, allowing the isolation of west Indian Ocean monsoonal component in regional rainfall. In this study we investigate key questions regarding the paleoclimate history of the northwestern Madagascan summer monsoon. How did the monsoon respond to climate forcing over the last two millennia? Can these changes be attributed to zonal or meridional controls?

To address the question of whether past precipitation variations in the wet Indian Ocean region have varied synchronously in-phase between the hemispheres, synchronously anti-phase or asynchronously, high-resolution precisely-dated records of past climates are needed. Stalagmites are ideal paleoclimate archives for this task, as their high resolution and precise U-Th dating provide records from both the northern and southern hemispheres, and can therefore distinguish the potential phasing of recent climate changes.

From Anjohibe cave in northwestern Madagascar (15°32′S, 46°53′E), we use stalagmite AB2 from Burns et al. (2016). For this study AB2 was sampled at much higher resolution to create a quasi-annual record of paleoclimate variability. Anjohibe cave is in the Narinda karst region in the northwest of Madagascar, 73 km northeast of Mahajanga. The Narinda karst is an Eocene limestone topped with dolomite. The surface is primarily rolling grassy hills of moderate relief with sparse endemic satra palms and other trees adapted to the highly seasonal rainfall. Dry mesic woodlands and forest patches occur in wetter areas. The carbonate overburden at Anjohibe is almost 100 m thick and grades from pure limestones at the base through calcareous dolomites to pure dolomites at the top (Gebauer et al., 1993). The temperature of the 5.3 km network of passages varies between 24.5 and 26 °C (Voarintsoa et al., 2017). We noted no soda straws during fieldwork. Drips are for the most part highly seasonal, with active drips only during and shortly after the rainy season.

Whereas the original low resolution record focused on $\delta^{13}C$ as a proxy for vegetation change, our new high-resolution $\delta^{18}O$ time series serves as a record of past hydrologic variability over northwestern Madagascar. Anjohibe cave is well suited to recording changes in the northwest Madagascan monsoon. Rainfall in the region is dominated by the austral summer monsoon with 85% of the yearly rainfall total of 1486 mm falling between December and March (rainfall data from the nearby city of Mahajanga). 62% of annual rainfall and the majority of extreme rainfall events >100 mm day^{-1} are concentrated in January and February, the peak monsoon season (J. F. Griffiths and Ranaivoson, 1972). In contrast Mahajanga receives just 140 mm during the austral spring (SON) when the IOD is at its most variable. Therefore, speleothems from Anjohibe should serve as excellent records of summer monsoon variability in Madagascar and the southwest Indian Ocean region.

2. Methods

In addition to the eight U-Th ages and three isochrons that determined the original published chronology of stalagmite AB2 (Burns et al., 2016), we added nine new U-Th ages to help further constrain the age model (Table 1). U-Th dating samples weighing 135–200 mg were prepared and analyzed at the Massachusetts Institute of Technology. Samples were combined with a ^{229}Th-^{233}U-^{236}U tracer, digested and purified via iron coprecipitation and ion exchange chromatography. U and Th were analyzed on separate aliquots using a Nu Plasma II-ES multi-collector ICP-MS equipped with a CETAC Aridus II desolvating nebulizer.

U-Th ages were calculated using the half-lives of Cheng et al. (2013) and Jaffey et al. (1971) and an initial $^{230}Th/^{232}Th$ ratio of $17 \pm 8.5 \times 10^{-6}$ based on isochron data and constraints from near-modern deposits at the top of the stalagmite (Burns et al., 2016). The stalagmite age model was constructed using the OxCal Bayesian modelling software and a Poisson process depositional model (P-Sequence) (Bronk Ramsey, 2008) using all seventeen U-Th ages plus additional assumptions of a zero age at the stalagmite top (2014 CE) and a boundary shift at 120.2 mm, in line with a change in stalagmite texture (Fig. 2).

We sampled stalagmite AB2 for stable isotope analysis at higher resolution with samples drilled from a cut and polished slab. Subsamples were taken at intervals varying from 0.2 to 2 mm depending on stalagmite growth rate. This increased the temporal resolution from approximately decadal to quasi-annual (<1 year at the top of the stalagmite, and approximately 2 years towards the base). The lack of visible annual layers prevents a precise annual chronology. Stable oxygen and carbon isotope ratios were determined using a Finnigan Delta Plus XL ratio mass spectrometer with a Kiel Carbonate Device at the University of Massachusetts, Amherst. Results are reported as per mil relative to the Vienna PeeDee Belemnite (VPDB) standard. Reproducibility of standard materials is 0.1‰ for $\delta^{18}O$ and 0.05‰ for $\delta^{13}C$. To determine the mineralogy of stalagmite AB2, we conducted X-ray diffraction (XRD) analyses on 20 subsamples drilled adjacent to the stable

Table 1
U-Th dating results.

Sample ID	Transect distance (mm)	^{238}U [a] (ng/g)	±2σ	^{232}Th [a] (pg/g)	±2σ	$\delta^{234}U$ [b] (per mil)	±2σ	$^{230}Th/^{238}U$ (activity)	±2σ	$^{230}Th/^{232}Th$ (atomic $\times10^{-6}$)	±2σ	Uncorr. Age [c] (yr)	±2σ	Corr. Age [d] (yr)	±2σ	$\delta^{234}U$ initial [e] (per mil)	±2σ	Year CE [d]	±2σ
AB2-9.5	9.5	7940	160	1204	25	−9.1	1.4	0.0002539	0.0000099	27	1	28	1	10	9	−9.1	1.4	2005	9
AB2-24.6	24.6	9260	400	186	8	−10.3	0.8	0.0008654	0.0000084	685	28	95	1	93	2	−10.3	0.8	1923	2
AB2-44.6	44.6	9310	210	2744	56	−10.0	0.6	0.0013984	0.0000092	75	0.5	154	1	119	17	−10.0	0.6	1897	17
AB2-62	62.0	9160	180	496	11	−10.0	0.6	0.001484	0.000020	436	7	164	2	157	4	−10.0	0.6	1858	4
AB2-87.8	87.8	13710	440	1778	36	−8.4	0.9	0.001984	0.000011	243	1.3	218	1	203	8	−8.4	0.9	1813	8
*AB2-114**	*114.0*	*183*	*4*	*485*	*11*	*−10.0*	*2.1*	*0.01252*	*0.00070*	*75*	*4*	*1387*	*78*	*1080*	*170*	*−10.0*	*2.1*	*935*	*170*
AB2-150	150.0	7950	160	2867	57	−12.8	1.4	0.004181	0.000018	184	0.7	463	2	420	21	−12.8	1.4	1595	21
AB2-190	190.0	5560	110	1067	22	−3.0	1.3	0.004359	0.000036	361	3	478	4	455	12	−3.0	1.3	1560	12
AB2-241.2	241.2	4327	4328	23850	570	−6.7	0.6	0.009331	0.000059	27	0.4	1029	7	380	330	−6.7	0.6	1640	330
AB2-298.1	298.1	6750	140	1205	29	−8.7	1.2	0.005300	0.000023	471	7	585	3	564	11	−8.7	1.2	1452	11
AB2-455	455.0	3561	3561	4157	83	−7.8	1.3	0.008719	0.000054	119	0.7	963	6	825	69	−7.8	1.2	1190	69
*AB2-556**	*556.0*	*1096*	*22*	*274*	*6*	*−7.1*	*2.7*	*0.01076*	*0.00012*	*683*	*10*	*1188*	*14*	*1159*	*20*	*−7.1*	*2.7*	*856*	*20*
AB2-560.1	560.1	2048	2048	179	9	−3.0	1.7	0.010076	0.000066	1832	90	1108	7	1097	9	−3.0	1.7	919	9
AB2-631.1	631.1	2702	2702	809	18	−1.8	0.9	0.010750	0.000058	570	6	1181	6	1146	19	−1.8	0.9	870	19
AB2-674	674.0	10710	220	281	7	−6.7	3.0	0.010318	0.000053	6252	94	1138	7	1135	7	−6.6	3.0	880	7
AB2-835	835.0	8780	180	331	7	−3.8	0.6	0.011386	0.000042	4789	47	1253	5	1249	5	−3.8	0.5	766	5
AB2-897.6	898.6	7620	150	405	12	−3.85	0.58	0.012348	0.000045	3689	83	1360	5	1354	6	−3.86	0.58	662.1	6
AB2-988	995.6	8220	160	943	19	0.4	7.9	0.014025	0.000084	1943	13	1540	15	1526	17	0.4	7.9	489	17
AB2-1066.1	1068.6	4177	4178	3495	71	−3.1	1.5	0.01542	0.00011	292.5	2.3	1700	13	1602	51	−3.2	1.5	414	51

Decay constants for ^{230}Th and ^{234}U are from Cheng et al. (2013); decay constant for ^{238}U is from Jaffey et al. (1971).

* Data in italics are thought to have experienced uranium loss and are not included in the age model.

[a] Reported errors for ^{238}U and ^{232}Th concentrations are estimated to be ±1% due to uncertainties in spike concentration; analytical uncertainties are smaller.

[b] $\delta^{234}U = ([^{234}U/^{238}U]_{activity} - 1) \times 1000$.

[c] "Uncorrected" indicates that no correction has been made for initial ^{230}Th.

[d] Ages are corrected for detrital ^{230}Th assuming an initial $^{230}Th/^{232}Th$ of $(17 \pm 8.5) \times 10^{-6}$.

[e] $\delta^{234}U_{initial}$ corrected was calculated based on ^{230}Th age (T), i.e., $\delta^{234}U_{initial} = \delta^{234}U_{measured} \times e^{\lambda 234 * T}$, and T is corrected age.

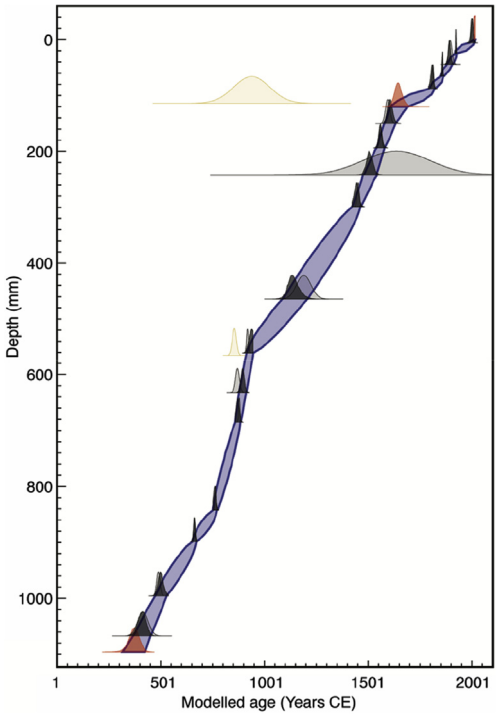

Fig. 2. AB2 age model (blue) constructed in OxCal using 17 U-Th ages. Original U-Th ages with 2σ errors in light grey, distribution of modelled ages at original age depths in dark grey, additional model assumptions in red: depth at base of stalagmite, depth of growth rate change based on textural shift in the stalagmite, data and age (2014 CE) of the top of the stalagmite to prevent a modelled positive age. Yellow ages are outliers not used in the age model (Burns et al., 2016). (For interpretation of the references to colour in this figure legend, the reader is referred to the web version of this article.)

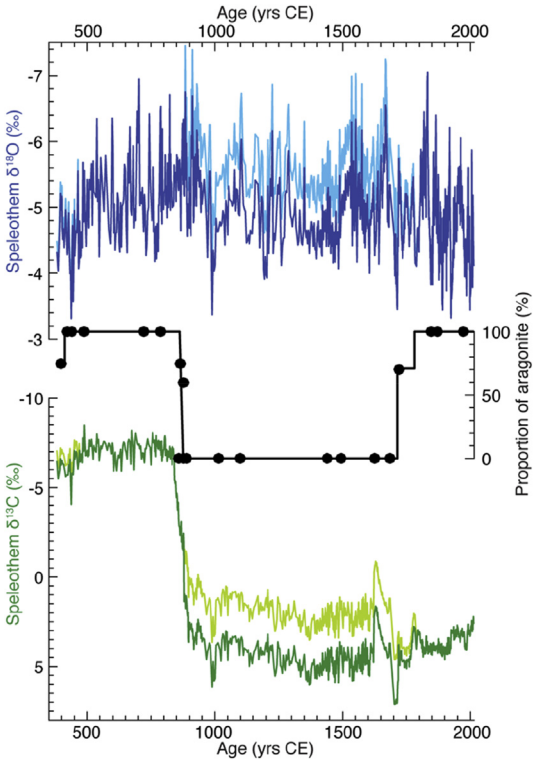

Fig. 3. Stable isotope and X-ray diffraction results from stalagmite AB2. Top: $\delta^{18}O$ (‰) uncorrected (light blue) and corrected (dark blue) for mineralogy. Middle: X-ray diffraction estimates of aragonite versus calcite percentage (black circles) with modelled mineralogy (black line) determined using Sr/Ca ratio transitions. Bottom: $\delta^{13}C$ (‰) uncorrected (light green) and corrected (dark green) for mineralogy.

isotope transect. XRD analyses were conducted on a PANalytical X'Pert PW1821 X-ray diffractometer at the University of Massachusetts, Amherst.

3. Results

XRD results indicate that stalagmite AB2 is composed of both calcite and aragonite (Fig. 3). Within the spatial and detection limits of XRD analysis the stalagmite is mostly monomineralic, composed of either calcite or aragonite, although we note that micrometer-scale relicts due to incomplete transformation may be present. Mixed calcite and aragonite signals arise in two narrow intervals at the base of the stalagmite between 1071 and 1097 mm (382–470 CE), and towards the top at 92–106 mm (1718–1790 CE). Visual inspection suggests that the section between 670 and 700 mm (860–880 CE) is likely composed of thin alternating calcite and aragonite layers. Two dates at 560 and 631 mm appear to be 100 years older than would be expected from a simple linear age model for the stalagmite, and a date at 556 mm is out of stratigraphic order. Each of these samples have lower U concentrations than adjacent samples (~2000 ng/g for the samples at 560 and 631 mm, and 1096 ng/g for the sample at 556 mm, compared to 3500 ng/g in adjacent samples), consistent with possible U loss. As the two dates at 560 and 631 mm are still in stratigraphic order, they are retained in the age model, and only the out-of-order date at 556 mm is rejected. Good reproducibility of the dating and isotopic time series between stalagmites AB2 and AB3 in Burns et al. (2016) suggests that if any recrystallization occurred, it has played a minor role in the age model and stable isotope records.

To test the impacts of changing mineralogy and potential recrystallization, the Sr/Ca ratio stalagmite AB2 was scanned using ITRAX X-ray fluorescence core-scanning (Finné et al., 2015). The trace element scanning was conducted on the opposite stalagmite face to the stable isotope transect but at the same resolution (0.2 or 1 mm). Results indicate that aragonite sections have Sr/Ca ratios three times higher than calcite sections (0.00015 vs 0.00005 (counts per second per milliamp/counts per second per milliamp)), consistent with the contrasting partition coefficients for Sr into aragonite versus calcite (Wassenburg et al., 2016). Areas of suspected mixed mineralogy from XRD analysis contain an intermediate Sr/Ca ratio. Sr/Ca transitions from low (calcite) to high (aragonite) are typically sharp (Perrin et al., 2014). We therefore used the Sr/Ca record to delineate mineralogy changes and create a mineralogy-corrected stable isotope record (Fig. 3). We converted calcite stable isotope values to their aragonite equivalent using a correction of 0.75‰ for $\delta^{18}O$ and +2.5‰ for $\delta^{13}C$ (Kim et al., 2007; Kim and O'Neil, 1997; Tarutani et al., 1969), with a proportional correction during the mixed mineralogy sections. The updated $\delta^{13}C$ results enhance the conclusions of Burns et al. (2016), with the $\delta^{13}C$ shift around 900 CE now 10.5‰ rather than the 8.0‰ previously reported in stalagmite AB2.

Speleothem $\delta^{18}O$ varies between −3.3 and −7‰ with higher values at the beginning and end of the record and lower values in between. The mineralogy-corrected record reveals a period of high values in the middle of the record between 1000 and 1500 years CE. Spectral analysis reveals no significant periodicities in the speleothem $\delta^{18}O$ record. Wavelet analysis does reveal some high frequency periodicity but there is no consistent frequency through long periods of time. Autocorrelation shows a peak at 142 years significant at 90% confidence, but the lack of correspondence with other techniques caution us against assigning undue influence to this potential periodicity.

4. Discussion

We interpret increases (or decreases) in stalagmite $\delta^{18}O$ as indicators of decreases (or increases) in the intensity of the convective system and rainfall in the northwestern Madagascan monsoon. It is known that increasing convergence of water vapor is a key contributor to the amount effect, which is likely closely related to the total precipitation amount. In Madagascar, the paucity of the instrumental record combined with the precision of the age model prevent direct confirmation of the amount effect. However, theoretical and mechanistic considerations (Bony et al., 2008; Dansgaard et al., 1993; Risi et al., 2008; Rozanski et al., 1993) regarding tropical precipitation (Kurita et al., 2009; LeGrande and Schmidt, 2009), are well established at tropical cave sites, leading us to interpret the amount effect as a dominant control of speleothem $\delta^{18}O$ (Burns et al., 2002, 1998; Lachniet, 2009; Partin et al., 2007; X. Wang et al., 2004).

Other potential controls on speleothem $\delta^{18}O$ include changes in rainfall seasonality or source, moisture recycling, upstream rainout, and cave temperature. Northwest Madagascar has a highly seasonal precipitation pattern, dominated in both amount and intensity by strong convective ITCZ monsoon rainfall during the austral summer. Summer rainfall has a single moisture source, the equatorial west Indian Ocean. There is unlikely to be any $\delta^{18}O_{precip}$ change arising from changing the source of moisture. The coastal western equatorial Indian Ocean, offshore western equatorial Indian Ocean and Mozambique channel have similar $\delta^{18}O_{sw}$ values (LeGrande and Schmidt, 2006). Close proximity of Anjohibe to the coast reduces the influence of moisture recycling and provides a short vapor transport path (Lee et al., 2009). Despite recent cave collapses which have enhanced cave ventilation, temperature variation inside Anjohibe is low both spatially (24.5–26 °C) (Voarintsoa et al., 2017) and temporally, with a year-round range of <3.5 °C in the MMAT external to the cave. This reduces the potential for both temperature driven variations in fractionation inside the temperature-buffered cave and altered cave ventilation. The highly seasonal nature of rainfall at Anjohibe is driven by the orography and therefore the potential $\delta^{18}O$ influence from changing rainfall seasonality through time is minimal. In other words increasing easterly moisture to Madagascar would not increase rainfall at Anjohibe. Therefore, it is reasonable to embrace the amount effect back past the limits of the instrumental record.

4.1. Decadal scale variability

The decadal scale contains the highest proportion of $\delta^{18}O$ variability (Fig. 3): the range of $\delta^{18}O$ at the decadal scale is 3.4‰ about the centennial means, while centennial variability is less than 1‰. It is difficult to identify the causes of decadal variability, be it local effects, regional teleconnections or stochastic processes, due to poor instrumental records and age model precision. For example, we see no correlation between speleothem $\delta^{18}O$ and possible upstream decadal frequency climate drivers such as the Pacific Decadal Oscillation (NCEI Index based on (Huang et al., 2015)), Atlantic Multidecadal Oscillation (Enfield et al., 2001), or solar irradiance (Coddington et al., 2016). The lack of correlation is not surprising as there are no demonstrated stationary relationships between these regional drivers and either west Indian Ocean SSTs or precipitation in the modern climate (Konecky et al., 2014; Nakamura et al., 2009; Zinke et al., 2009). This result indicates a need for annually resolved precipitation records such as laminated speleothems and corals to help constrain regional climate mechanisms at the decadal scale.

4.2. Multi-decadal scale variability

To investigate multi-decadal to centennial scale climate variability in the western Indian Ocean, the Anjohibe speleothem $\delta^{18}O$ record was compared to a high-resolution speleothem $\delta^{18}O$ record from Cave Defore in Oman, located at 16°N and 53°E (Burns et al., 2002) and thus an excellent Northern Hemisphere counterpart to AB2. Both records were band-pass filtered to between 50 and 300 years to remove decadal variability and long term trends. The filtered Anjohibe record shows a range of 1.4‰, close to 40% of the total $\delta^{18}O$ variability. An alternating wet and dry pattern of 9 or 10 cycles occurs at both locations over the last 800 years (Fig. 4). The two filtered records have a correlation of $r = 0.27$ ($n = 319$) over the entire length of the record, and a median r value of 0.76 when using a 50-year moving window, suggesting a highly in-phase relationship. Due to high autocorrelation above 0.96 in both filtered records, p-values cannot be obtained. The mean 2σ age error in the Anjohibe age model is 16.6 years, while the Cave Defore record is layer counted with an error of ±5 layers by the base. U-Th ages are used to test the Cave Defore age model but not in its construction. Age model errors are therefore unlikely to change the phase of the two records. The approximate return time of the wet/dry cycles is 80–90 years. While there are no significant spectral peaks in the Anjohibe record around these periodicities, the Oman $\delta^{18}O$ record contains a peak at 97 years. There are two exceptions to the high in-phase correlation: a period from 1643 to 1687 (discussed below) and the 20th century.

The dominant in-phase relationship between Madagascar and Oman is unexpected. Speleothem precipitation records from Oman have been demonstrated to be sensitive to high northern latitude climate variability, and interpreted as indicating north-south movements in mean ITCZ location on multiple timescales (Fleitmann et al., 2003, 2004). If the multi-decadal scale variability of rainfall recorded in the two regions is the result of changes in mean ITCZ position, we would expect a north-south anti-phase relationship in precipitation amount. The observed pattern instead fits with the idea of expansion and contraction of the tropical rain belt rather than translation (Denniston et al., 2016; Yan et al., 2015).

A notable exception to the in-phase relationship occurs at 1643–1687 when a wet anomaly in Madagascar and a dry anomaly in Oman create an anti-phase relationship. The timing of this anomaly is coincident with a minimum in global temperatures during the Little Ice Age associated with a volcanic-solar downturn (PAGES 2k Consortium, 2013). Under the schema of north-south ITCZ translation, shifts in the regional ITCZ may reflect a differential response of each hemisphere to changing global temperatures owing to an imbalance in land surface area. Even symmetric climate forcing such as solar variability may then cause an asymmetrical response. Volcanic aerosol forcing can be symmetrical or asymmetrical but is likely to cause an asymmetric ITCZ response in the tropics (Colose et al., 2016). It is therefore apparent that relatively large meridional forcing may be able to override the observed in-phase relationship. However, this mechanism does not seem to apply at other times of high stratospheric sulphate aerosol concentration and low total solar irradiance: e.g. 1250–1350CE (Gao et al., 2008), with the caveat that the dating uncertainty during this period is larger. As the multi-decadal to centennial scale forcing on tropical rainfall is relatively weak, it remains an open question as to what happens at orbital timescales when asymmetric forcing of summer insolation is very large.

The second out of phase anomaly occurs during the 20th century. A wet 1950s and 60s, followed by a thirty-year dry period that peaks in the 1970s-1980s in the AB2 record matches Africa-wide precipitation, suggesting in-phase cross-equatorial precipitation (Nash et al., 2016; Nicholson, 2001). The anomaly is likely related to

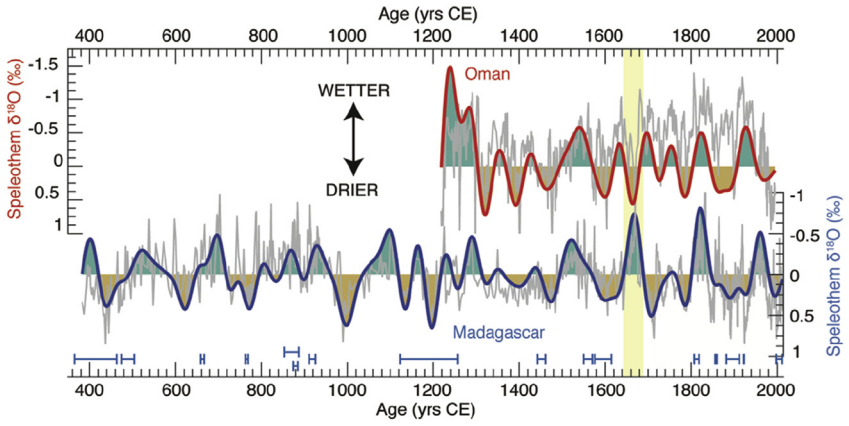

Fig. 4. Comparison of the Cave Before, Oman (Burns et al., 2002) (red) and Anjohibe, Madagascar (this study) (blue) speleothem $\delta^{18}O$ records band pass filtered to between 50 and 300 years. Grey lines indicate the prefiltered $\delta^{18}O$ records, while green and brown shading show periods with wetter and drier than average conditions respectively. Dates from stalagmite AB2 with 2σ error are shown with blue bars. No dates are included for the Oman record as the stalagmite S3 was dated using layer counting. Shaded yellow area between 1643 and 1687 denotes a period of anomalous anti-phase behavior between the two records. (For interpretation of the references to colour in this figure legend, the reader is referred to the web version of this article.)

the positive $\delta^{18}O$ (drying) trend in the Oman record, which may reflect a reduction in the land-sea thermal contrast as the ocean warmed faster than the land (Burns et al., 2002).

4.3. Centennial scale variability

The Anjohibe speleothem $\delta^{18}O$ record has large high-frequency variability with only minor changes in long-term (centennial- to millennial-scale) mean, suggesting that monsoonal rainfall has been largely consistent in absolute terms over the past two millennia. Statistically significant changes in the long-term mean, however, have occurred. To investigate these changes we performed a Bayesian change point analysis (BCPA) to identify points in the $\delta^{18}O$ record where there are significant changes in the mean $\delta^{18}O$ and/or $\delta^{18}O$ variability (Partin et al., 2015; Ruggieri, 2013). We conducted 10,000 analyses on a regularly spaced, 2-year resolution, synthetic proxy record using modelled time intervals with zero $\delta^{18}O$ gradient to produce a series of 'change points' at which significant changes in speleothem $\delta^{18}O$ occur.

The outcomes of our BCPA analyses show a maximum likelihood of 7 change points (Table 2), with 98% of outcomes evidencing 6–8 change points. Three of the seven change points have a $\delta^{18}O$ change of >0.45‰ and are supported by at least 99.9% of model outcomes. Four smaller shifts have a $\delta^{18}O$ change of >0.1‰ and are supported by more than 70% of model outcomes. There are additional change points with support of less than 20% of the individual outcomes, which influence the modelled mean by minor amounts. The total change in mean $\delta^{18}O$ explained by BCPA is 0.92‰, ~25% of the total variability in the $\delta^{18}O$ record. BCPA also produces a modelled mean between change-points, which indicates a series of multi-centennial long high and low $\delta^{18}O$ periods, which we interpret as periods of relatively wet and dry conditions in northwestern Madagascar. Three dry intervals occur in the record: prior to 481CE, between 967 and 1481CE and since 1883CE. Two wet intervals occurred between 487 and 945CE and 1495–1833CE (Fig. 5a).

Table 2
Location of seven $\delta^{18}O$ shifts detected in the Anjohibe speleothem record using Bayesian Change-Point Analysis. Top section: three large shifts with $\delta^{18}O$ > 0.45‰ supported by >99.9% of model outcomes. Bottom section: four smaller shifts with $\delta^{18}O$ > 0.1‰ supported by >70% of model outcomes.

95% Age Range (yr CE)	Modal Age (yr CE)	Change in $\delta^{18}O$ (‰)
481–487	481	−0.70
945–967	963	+0.53
1481–1495	1485	−0.45
771–821	781	−0.27
1295–1359	1295, 1351	+0.24
1595–1701	1695	+0.12
1833–1883	1837, 1867	+0.26

We compare the Anjohibe BCPA record with high-resolution proxy rainfall records from east African lakes. Lake records have a significantly larger catchment than speleothems and so integrate broader spatial regions. While the resolution of lake records can often be as high as or higher than that of speleothems due to varves and high accumulation rates, speleothem U-Th age models are typically more precise than the radiocarbon age models of lake deposits. Despite the diverse catchments and dating precision of speleothems and lakes, we have found good coherence between the records (Fig. 5d,e,f). An alternating sequence of dry and wet conditions is apparent in the Anjohibe speleothem record from Madagascar and the sediment core records from Lakes Challa and Naivasha from the Horn of Africa (Buckles et al., 2016; Tierney et al., 2013; Verschuren et al., 2000). Overall, three dry and two wet phases, with each individual complete phase lasting about 500 years, appear to characterize regional rainfall patterns in the tropical western Indian Ocean over the past 2000 years (Fig. 5).

Correlation between the Madagascar and Oman records at this timescale is mixed (Fig. 5b). Burns et al. (2002) and Fleitmann et al. (2004) demonstrate a dry period in Oman during the first half of LIA between 1320 and 1660. We note a wet period in the second half of the LIA record between 1680 and 1900. An anti-phase relationship exists with the Lake Edward paleoprecipitation record in the African Rift Valley (Fig. 5c), which agrees with the Horn-Rift rainfall dichotomy (Tierney et al., 2013) and extends the duration and spatial extent of this regional rainfall pattern.

4.4. Zonal and meridional controls on late holocene tropical precipitation

Here we investigate how different climate drivers may produce the surprising cross-equatorial symmetrical response in monsoon rainfall: local landmass sensible heating, Walker circulation variability, Indian Ocean Dipole dynamics, and west Indian Ocean SSTs. In addition to movement of the ITCZ, the monsoons are also influenced by local factors such as the sensible heating of

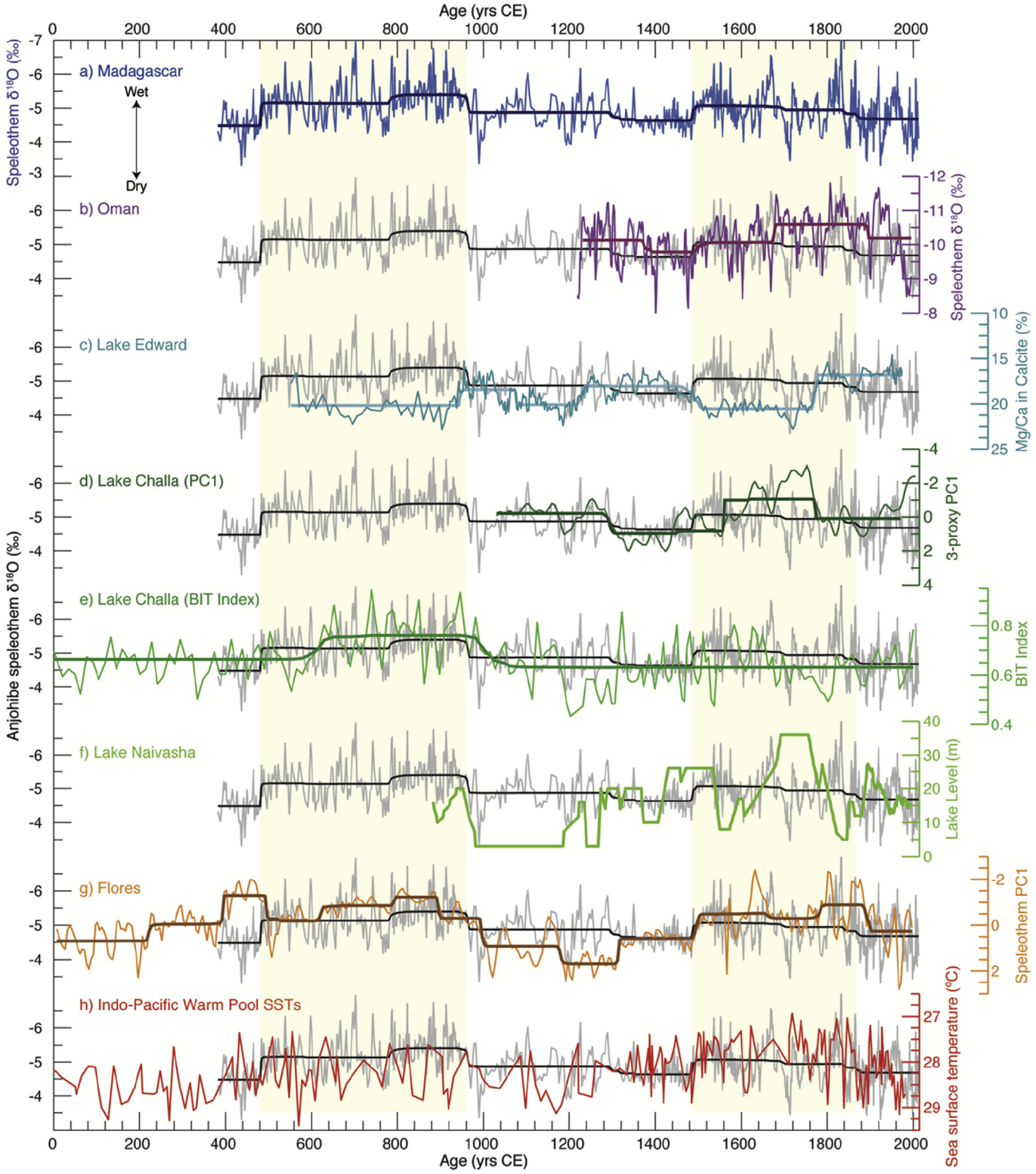

Fig. 5. Comparison of the Anjohibe speleothem $\delta^{18}O$ record (blue at top, grey in lower panels) with regional indicators of zonal and meridional tropical climate systems. b) Cave Defore, Oman (Burns et al., 2002) (purple), c) Lake Edward, Uganda/Democratic Republic of Congo (Russell and Johnson, 2007) (turquoise), d) Lake Challa, Tanzania/Kenya (Tierney et al., 2013) (dark green), e) Lake Challa, Tanzania/Kenya (Buckles et al., 2016) (green), f) Lake Naivasha, Kenya (Verschuren et al., 2000) (light green), g) Liang Luar Cave, Flores, Indonesia (Griffiths et al., 2016) (orange), h) Indo-Pacific Warm Pool SSTs (red) (Oppo et al., 2009). For each record where Bayesian Change Point Analysis with zero gradient was successful, darker lines are included to show the modelled mean. All records are oriented so that wet is up, with the exception of the Indo-Pacific Warm Pool, which is not a paleoprecipitation proxy.

landmasses that drives onshore convection. During the late Holocene, solar variability is symmetrical. If the impact of variable landmass sensible heating is able to locally override the impact of north-south ITCZ translation, then a symmetrical contraction and expansion of the tropical rain belt may result (Yan et al., 2015). This idea fits well with the multi-decadal in-phase rainfall relationship seen between Madagascar and Oman. However, this mechanism of tropical rain belt expansion and contraction should produce a tropics-equator-tropics tripole, where more (less) time spent at higher latitudes increases (decreases) precipitation at the extremes of the monsoon and decreases (increases) precipitation on the equator. Band pass filtered records of equatorial African precipitation show no systematic drying on the equator at this timescale, suggesting a more complicated regional precipitation response than meridionally forced expansion and contraction of the tropical rain belt.

Similarly, the multi-centennial coherency of west Indian Ocean precipitation does not fit with either north-south translation of the ITCZ or the tripole pattern of expansion and contraction of the tropical rain belt. While Yan et al. (2015) posited a meridionally forced tripole pattern, Denniston et al. (2016) suggest that both zonal and meridional climate drivers may be required for ITCZ contraction and expansion. A response of the zonal Walker circulation to meridional ITCZ forcing may drive regional precipitation. An increase in Pacific Walker circulation during the LIA has been inferred as a potential mechanism for the both the contraction of the ITCZ across the IPWP and an observed cross-Pacific anti-phase precipitation relationship during the LIA (M. L. Griffiths et al., 2016). However, enhanced Walker circulation (La Niña like state) would produce drier conditions in the west Indian Ocean, opposite to the wet conditions seen in the regional proxy records. Reduced Walker circulation would result in the El Niño like state observed in the regionally wet precipitation pattern in east Africa, but would require a decoupling of Indian and Pacific Walker circulation.

Atmospheric modelling studies suggest that low-frequency zonal variability in the Indian Ocean is related to changes in the intensity or frequency of the IOD rather than the underlying mean state (Konecky et al., 2014; Tozuka et al., 2007). However, the IOD is a much more seasonally locked climate mode than ENSO, with maximum impact during the austral spring (SON). Therefore, changes to IOD intensity or frequency are unlikely to influence all of the separate monsoon seasons seen in the region: Madagascar: JFM, Oman: JJA, East Africa: MAM and/or SON. Additionally, northwestern Madagascan rainfall is insulated from direct zonal interannual climate variability related to the IOD because the IOD primarily drives changes in easterly trade wind strength and the eastern massifs block trade wind derived precipitation.

Oceanic models predict lower frequency changes in the Indian Ocean related to the thermocline (Ashok et al., 2004), which suggests that oceanic changes may be responsible for changing regional precipitation. Warm west Indian Ocean SSTs would result in enhanced moisture evaporation, latent heat transport and convection, leading to greater rainfall in the west Indian Ocean. Higher SSTs might also contribute a higher frequency of tropical cyclone hits, adding additional depleted $\delta^{18}O$ to the karst system. This low frequency SST mechanism would serve to synchronize regional precipitation records despite the contrasting timing of rainy seasons in different hemispheres. Further it would give rise to an appearance of expansion and contraction of the tropical rain belt. However, warming of the oceans also reduces the land-sea thermal contrast, which may reduce monsoon strength (Burns et al., 2002). Contrasting responses to SST changes could explain why the Oman record does not match the Madagascan record at the centennial timescale in the first half of the LIA.

We now turn to the question of what might drive west Indian Ocean SST variability. The regionally coherent precipitation pattern resulting from a low frequency SST mode could result in one of three possible scenarios. First, a dipole pattern similar to the modern IOD, with cooler drier conditions in the eastern Indian Ocean, could have occurred. Such a pattern could be controlled by upstream Indonesian Throughflow behavior forcing the eastern Indian Ocean thermocline. West Indian Ocean precipitation records are anti-phased with Indo-Pacific Warm Pool (IPWP) SSTs (Fig. 5h) (Oppo et al., 2009; Tierney et al., 2013), but the role of the Pacific Ocean may obscure any Indian Ocean influence and it is uncertain if low frequency IOD modes influence East African precipitation amount (Konecky et al., 2014). Second, a basin-wide SST mode may produce in-phase SST variations. Modelling results suggest a low-frequency basin-wide SST mode does exist, at least at the decadal scale (Tozuka et al., 2007). Thirdly, there may be no cross-basin relationship. While a SST dipole exists for the IOD, models suggest it is not a required feature of interannual East African rainfall variability (Ummenhofer et al., 2009). Unfortunately, there are no tropical Indian Ocean SST records of sufficient (decadal) resolution that cover the past 2000 years with which to make direct comparisons and elucidate the relevant mechanisms at lower frequencies.

In the absence of appropriate SST records from the eastern Indian Ocean we investigate terrestrial precipitation records. We compare our Madagascan record to the 2000-year, high resolution, multiproxy, speleothem paleoprecipitation record from Liang Luar Cave, Indonesia (Fig. 5g) (M. L. Griffiths et al., 2016). The two records show a remarkable in-phase relationship with Madagascar. Both records show with two multi-century wet phases: the 16th–18th centuries, which matches several west Indian Ocean precipitation records, and the 6th–10th centuries. Two drier periods occurred in the 11th–15th centuries and in the 20th century. This result is also surprising as under a zonal mechanism we might expect an anti-phase east-west cross basin relationship, as observed in the Pacific (M. L. Griffiths et al., 2016), and so some doubt is cast onto the idea of a zonal dipole at the centennial scale. However, it may be that the Flores record responds to Pacific climate dynamics and changes in the IPWP to a far greater extent than it does to the Indian Ocean (M. L. Griffiths et al., 2016; Konecky et al., 2014), and therefore does not represent a true point of comparison for the east Indian Ocean. There is a need for unambiguous eastern Indian Ocean precipitation and SST records so that more definitive conclusions to be made about the competing influences of zonal and meridional mechanisms in controlling tropical precipitation variability during the late Holocene.

5. Conclusions

Our new $\delta^{18}O$ record from stalagmite AB2 from Anjohibe, northwestern Madagascar, provides a quasi-annual precisely dated record of past rainfall variability in the Madagascan monsoon. The largest variability in the record is at the decadal scale, shows little correlation with decadal-scale climate indices, and has no pronounced cyclicity. At multi-decadal timescales, the Madagascan record is primarily in-phase with its northern hemisphere speleothem counterpart from Oman. This is a surprising result as the Omani record is believed to respond to northern hemisphere climate forcing, and therefore a meridional dipole of tropical rainfall related to movements of the ITCZ might be expected. The two exceptions to the in-phase relationship occur during the mid-17th century and the 20th century, when there was stronger global climate forcing. At the centennial timescale there are good correlations between our record and paleoprecipitation records from the Horn of Africa, notably with wet conditions prevalent between the 16th and 18th centuries.

The cause of this regional coherency is unclear and may be related to either zonal or meridional forcing, or more likely, both. The multi-decadal rainfall pattern fits well but not perfectly with the idea of tropical rain belt expansion and contraction. This pattern may derive from symmetrical increases and decreases in landmass sensible heating that locally override the global ITCZ north-south translation as a response to the changing interhemispheric temperature gradient. At the centennial scale, a zonal Indian Ocean mechanism may change regional rainfall through altered moisture flux to the atmosphere. Given 1) the asynchronous rainfall seasons in the region and 2) the orographic insulation of the Anjohibe site from changes in IOD frequency, year-round SST changes are a plausible mechanism for changing the total amount of monsoonal rainfall. In the absence of suitable high resolution SST or paleoprecipitation records from the eastern Indian Ocean it is not yet possible to test basin-wide behavior and potential driving mechanisms. A fuller understanding of Indian Ocean low frequency climate behavior is required to help make more concrete predictions regarding future regional rainfall in this socio-economically vulnerable region.

Acknowledgements

DM acknowledges support from NSF award EAR-1439559 and the MIT Ferry Fund. Fieldwork in Madagascar was conducted under a collaborative accord for paleobiological and paleoclimatological research between the University of Antananarivo and the University of Massachusetts (Department of Anthropology and Department of Geosciences). We greatly appreciate the support and cooperation of the Madagascar Ministry of Art and Culture, Ministry of Mines and Petroleum, and Ministry of Higher Education and Scientific Research in sample collection.

References

Abram, N.J., Gagan, M.K., Cole, J.E., Hantoro, W.S., Mudelsee, M., 2008. Recent intensification of tropical climate variability in the Indian Ocean. Nat. Geosci. 1, 849–853. http://dx.doi.org/10.1038/ngeo357.

Abram, N.J., Gagan, M.K., Liu, Z., Hantoro, W.S., McCulloch, M.T., Suwargadi, B.W., 2007. Seasonal characteristics of the Indian Ocean dipole during the holocene epoch. Nature 445, 299–302. http://dx.doi.org/10.1038/nature05477.

Ashok, K., Chan, W.L., Motoi, T., Yamagata, T., 2004. Decadal variability of the Indian Ocean dipole. Geophys. Res. Lett. 31 http://dx.doi.org/10.1029/2004GL021345.

Ashok, K., Guan, Z., Yamagata, T., 2003. A look at the relationship between the ENSO and the Indian ocean dipole. J. Meteorol. Soc. Jpn. 81, 41–56. http://dx.doi.org/10.2151/jmsj.81.41.

Ault, T.R., Cole, J.E., Evans, M.N., Barnett, H., Abram, N.J., Tudhope, A.W., Linsley, B.K., 2009. Intensified decadal variability in tropical climate during the late 19th century. Geophys. Res. Lett. 36 http://dx.doi.org/10.1029/2008GL036924.

Ayliffe, L.K., Gagan, M.K., Zhao, J.-X., Drysdale, R.N., Hellstrom, J.C., Griffiths, M.L., Pierre, E.S., Hantoro, W.S., Cowley, J., Scott-Gagan, H., Suwargadi, B.W., 2013. Fluctuations of the Australasian monsoon on precessional and millennial timescales during the last deglaciation. Nat. Commun. 4, 2908. http://dx.doi.org/10.1038/ncomms3908.

Black, E., Slingo, J., Sperber, K.R., 2003. An observational study of the relationship between excessively strong short rains in coastal East Africa and Indian Ocean SST. Mon. Weather Rev. 131, 74–94. http://dx.doi.org/10.1175/1520-0493(2003)131<0074:AOSOTR>2.0.CO;2.

Bony, S., Risi, C., Vimeux, F., 2008. Influence of convective processes on the isotopic composition (δ18O and δD) of precipitation and water vapor in the tropics: 1. Radiative-convective equilibrium and Tropical Ocean–Global Atmosphere–Coupled Ocean-Atmosphere Response Experiment (TOGA-COARE) simulations. J. Geophys. Res. 113 http://dx.doi.org/10.1029/2008JD009942.

Broccoli, A.J., Dahl, K.A., Stouffer, R.J., 2006. Response of the ITCZ to northern hemisphere cooling. Geophys. Res. Lett. 33, L01702. http://dx.doi.org/10.1029/2005GL024546.

Bronk Ramsey, C., 2008. Deposition models for chronological records. Quat. Sci. Rev. 27, 42–60. http://dx.doi.org/10.1016/j.quascirev.2007.01.019.

Brook, G.A., Rafter, M.A., Railsback, L.B., Sheen, S.-W., Lundberg, J., 1999. A high-resolution proxy record of rainfall and ENSO since AD 1550 from layering in stalagmites from Anjohibe Cave, Madagascar. Holocene 9, 695–705. http://dx.doi.org/10.1191/095968399677907790.

Brown, E.T., Johnson, T.C., 2005. Coherence between tropical East African and South American records of the little ice age. Geochem. Geophys. Geosyst. 6 http://dx.doi.org/10.1029/2005GC000959.

Buckles, L.K., Verschuren, D., Weijers, J.W.H., Cocquyt, C., Blaauw, M., Sinninghe Damsté, J.S., 2016. Interannual and (multi-)decadal variability in the sedimentary BIT index of Lake Challa, East Africa, over the past 2200 years: assessment of the precipitation proxy. Clim. Past 12, 1243–1262. http://dx.doi.org/10.5194/cp-12-1243-2016.

Burns, S.J., Fleitmann, D., Mudelsee, M., Neff, U., Matter, A., Mangini, A., 2002. A 780-year annually resolved record of Indian Ocean monsoon precipitation from a speleothem from south Oman. J. Geophys. Res. 107 http://dx.doi.org/10.1029/2001JD001281.

Burns, S.J., Godfrey, L.R., Faina, P., McGee, D., Hardt, B., Ranivoharimanana, L., Randrianasy, J., 2016. Rapid human-induced landscape transformation in Madagascar at the end of the first millennium of the common Era. Quat. Sci. Rev. 134, 92–99. http://dx.doi.org/10.1016/j.quascirev.2016.01.007.

Burns, S.J., Matter, A., Frank, N., Mangini, A., 1998. Speleothem-based paleoclimate record from northern Oman. Geology 26, 499. http://dx.doi.org/10.1130/0091-7613(1998)026<0499:SBPRFN>2.3.CO;2.

Cheng, H., Lawrence Edwards, R., Edwards, R.L., Shen, C.-C., Polyak, V.J., Asmerom, Y., Woodhead, J., Hellstrom, J.C., Hellstrom, J., Wang, Y., Kong, X., Spötl, C., Wang, X., Calvin Alexander Jr., E., 2013. Improvements in 230Th dating, 230Th and 234U half-life values, and U–Th isotopic measurements by multi-collector inductively coupled plasma mass spectrometry. Earth. Planet. Sc. Lett. 371–372, 82–91. http://dx.doi.org/10.1016/j.epsl.2013.04.006.

Coddington, O., Lean, J.L., Pilewskie, P., Snow, M., Lindholm, D., 2016. A solar irradiance climate data record. Bull. Am. Meteorol. Soc. 97, 1265–1282. http://dx.doi.org/10.1175/bams-d-14-00265.1.

Colose, C.M., LeGrande, A.N., Vuille, M., 2016. Hemispherically asymmetric volcanic forcing of tropical hydroclimate during the last millennium. Earth Syst. Dyn. 7, 681–696. http://dx.doi.org/10.5194/esd-7-681-2016.

Cross, M., 2015. PySPLIT: a package for the generation, analysis, and visualization of HYSPLIT air parcel trajectories. In: Proc. of the 14th Python in Science Conf, pp. 137–142.

Dansgaard, W., Johnsen, S.J., Clausen, H.B., Dahl-Jensen, D., Gundestrup, N.S., Hammer, C.U., Hvidberg, C.S., Steffensen, J.P., Sveinbjörnsdottir, A.E., Jouzel, J., Bond, G., 1993. Evidence for general instability of past climate from a 250-kyr ice-core record. Nature 364, 218–220. http://dx.doi.org/10.1038/364218a0.

Denniston, R.F., Asmerom, Y., Lachniet, M., Polyak, V.J., Hope, P., An, N., Rodzinyak, K., Humphreys, W.F., 2013. A last glacial maximum through middle holocene stalagmite record of coastal Western Australia climate. Quat. Sci. Rev. 77, 101–112. http://dx.doi.org/10.1016/j.quascirev.2013.07.002.

Denniston, R.F., Ummenhofer, C.C., Wanamaker, A.D., Lachniet, M.S., Villarini, G., Asmerom, Y., Polyak, V.J., Passaro, K.J., Cugley, J., Woods, D., Humphreys, W.F., 2016. Expansion and contraction of the Indo-Pacific tropical rain belt over the last three millennia. Sci. Rep. 6, 34485. http://dx.doi.org/10.1038/srep34485.

Enfield, D.B., Mestas Nuñez, A.M., Trimble, P.J., 2001. The Atlantic Multidecadal Oscillation and its relation to rainfall and river flows in the continental U.S. Geophys. Res. Lett. 28, 2077–2080. http://dx.doi.org/10.1029/2000GL012745.

Eroglu, D., McRobie, F.H., Ozken, I., Stemler, T., Wyrwoll, K.-H., Breitenbach, S.F.M., Marwan, N., Kurths, J., 2016. See–saw relationship of the holocene East Asian–Australian summer monsoon. Nat. Commun. 7, 12929. http://dx.doi.org/10.1038/ncomms12929.

Finné, M., Kylander, M., Boyd, M., Sundqvist, H., Löwemark, L., 2015. Can XRF scanning of speleothems be used as a non-destructive method to identify paleoflood events in caves? Int. J. Speleol. 44, 17–23. http://dx.doi.org/10.5038/1827-806x.44.1.2.

Fleitmann, D., Burns, S.J., Mudelsee, M., Neff, U., Kramers, J., Mangini, A., Matter, A., 2003. Holocene forcing of the Indian monsoon recorded in a stalagmite from Southern Oman. Science 300, 1737–1739. http://dx.doi.org/10.1126/science.1083130.

Fleitmann, D., Burns, S.J., Neff, U., Mudelsee, M., Mangini, A., Matter, A., 2004. Palaeoclimatic interpretation of high-resolution oxygen isotope profiles derived from annually laminated speleothems from Southern Oman. Quat. Sci. Rev. 23, 935–945. http://dx.doi.org/10.1016/j.quascirev.2003.06.019.

Gao, C., Robock, A., Ammann, C., 2008. Volcanic forcing of climate over the past 1500 years: an improved ice core-based index for climate models. J. Geophys. Res. 113, D23111. http://dx.doi.org/10.1029/2008JD010239.

Gebauer, H., Guecke, W., Kaufmann, G., Laumanns, M., Rushin-Bell, C., Schoppl, T., Thrun, A., 1993. Report of the 1882 speleological expedition to Madagascar (Reserve Naturelle de Namoroka and Karst area of Narinda).

Global Facility for Disaster Reduction and Recovery, 2013. Country Profile: Madagascar.

Goddard, L., Graham, N.E., 1999. Importance of the Indian Ocean for simulating rainfall anomalies over eastern and southern Africa. J. Geophys. Res. 104, 19099–19116. http://dx.doi.org/10.1029/1999JD900326.

Griffiths, J.F., Ranaivoson, R., 1972. Madagascar. In: Griffiths, J.F. (Ed.), Climates of Africa. gbv.de.

Griffiths, M.L., Kimbrough, A.K., Gagan, M.K., Drysdale, R.N., Cole, J.E., Johnson, K.R., Zhao, J.-X., Cook, B.I., Hellstrom, J.C., Hantoro, W.S., 2016. Western Pacific hydroclimate linked to global climate variability over the past two millennia. Nat. Commun. 7 http://dx.doi.org/10.1038/ncomms11719.

Harou, A.P., Lajoie, R.F., Kniveton, D.R., Frogley, M.R., 2006. The influence of the Indian Ocean dipole mode on precipitation over the Seychelles. Int. J. Climatol. 26, 45–54. http://dx.doi.org/10.1002/joc.1239.

Hashizume, M., Terao, T., Minakawa, N., 2009. The Indian Ocean dipole and malaria risk in the highlands of western Kenya. Proc. Natl. Acad. Sci. 106, 1857–1862.

http://dx.doi.org/10.1073/pnas.0806544106.
Hastenrath, S., Polzin, D., Camberlin, P., 2004. Exploring the predictability of the "short rains" at the coast of East Africa. Int. J. Climatol. 24, 1333–1343. http://dx.doi.org/10.1002/joc.1070.
Haug, G.H., Hughen, K.A., Sigman, D.M., Peterson, L.C., Röhl, U., 2001. Southward migration of the intertropical convergence zone through the holocene. Science 293, 1304–1308. http://dx.doi.org/10.1126/science.1059725.
Huang, B., Banzon, V.F., Freeman, E., 2015. Extended reconstructed sea surface temperature version 4 (ERSST. v4). Part I: upgrades and intercomparisons. J. Clim. 28, 911–930. http://dx.doi.org/10.1175/jcli-d-14-00006.1.
Jaffey, A.H., Flynn, K.F., Glendenin, L.E., Bentley, W.C., Essling, A.M., 1971. Precision measurement of half-lives and specific activities of ^{235}U and ^{238}U. Phys. Rev. C 4, 1889–1906. http://dx.doi.org/10.1103/PhysRevC.4.1889.
Jury, M.R., Parker, B.A., Raholijao, N., Nassor, A., 1995. Variability of summer rainfall over Madagascar: climatic determinants at interannual scales. Int. J. Climatol. 15, 1323–1332. http://dx.doi.org/10.1002/joc.3370151203.
Jury, M.R., Pathack, B., 1991. A study of climate and weather variability over the tropical southwest Indian Ocean. Meteorl. Atmos. Phys. 47, 37–48. http://dx.doi.org/10.1007/BF01025825.
Jury, M.R., Pathack, B., Waliser, D., 1993. Satellite OLR and microwave data as a proxy for summer rainfall over sub-equatorial Africa and adjacent oceans. Int. J. Climatol. 13, 257–269. http://dx.doi.org/10.1002/joc.3370130303.
Kanner, L.C., Burns, S.J., Cheng, H., Edwards, R.L., 2012. High-latitude forcing of the South American summer monsoon during the last glacial. Science 335, 570–573. http://dx.doi.org/10.1126/science.1213397.
Kim, S.-T., O'Neil, J.R., Hillaire-Marcel, C., Mucci, A., 2007. Oxygen isotope fractionation between synthetic aragonite and water: influence of temperature and Mg^{2+} concentration. Geochim. Cosmochim. Acta 71, 4704–4715. http://dx.doi.org/10.1016/j.gca.2007.04.019.
Kim, S.T., O'Neil, J.R., 1997. Equilibrium and nonequilibrium oxygen isotope effects in synthetic carbonates. Geochim. Cosmochim. Acta 61, 3461–3475.
Konecky, B., Russell, J., Vuille, M., Rehfeld, K., 2014. The Indian Ocean zonal mode over the past millennium in observed and modeled precipitation isotopes. Quat. Sci. Rev. 103, 1–18. http://dx.doi.org/10.1016/j.quascirev.2014.08.019.
Kurita, N., Ichiyanagi, K., Matsumoto, J., Yamanaka, M.D., Ohata, T., 2009. The relationship between the isotopic content of precipitation and the precipitation amount in tropical regions. J. Geochem. Explor. 102, 113–122. http://dx.doi.org/10.1016/j.gexplo.2009.03.002.
Lachniet, M.S., 2009. Climatic and environmental controls on speleothem oxygen-isotope values. Quat. Sci. Rev. 28, 412–432. http://dx.doi.org/10.1016/j.quascirev.2008.10.021.
Lee, J.-E., Johnson, K., Fung, I., 2009. Precipitation over South America during the last glacial maximum: an analysis of the "amount effect" with a water isotope-enabled general circulation model. Geophys. Res. Lett. 36, L19701. http://dx.doi.org/10.1029/2009GL039265.
LeGrande, A.N., Schmidt, G.A., 2009. Sources of Holocene variability of oxygen isotopes in paleoclimate archives. Clim. Past 5, 441–455. http://dx.doi.org/10.5194/cp-5-441-2009.
LeGrande, A.N., Schmidt, G.A., 2006. Global gridded data set of the oxygen isotopic composition in seawater. Geophys. Res. Lett. 33, 15833. http://dx.doi.org/10.1029/2006GL026011.
Liu, Z., Otto-Bliesner, B., Kutzbach, J., Li, L., Shields, C., 2003. Coupled climate simulation of the evolution of global monsoons in the Holocene. J. Clim. 16, 2472–2490.
Macron, C., Richard, Y., Garot, T., Bessafi, M., Pohl, B., Ratiarison, A., Razafindrabe, A., 2016. Intraseasonal rainfall variability over Madagascar. Mon. Weather Rev. 144, 1877–1885. http://dx.doi.org/10.1175/mwr-d-15-0077.1.
Nakamura, N., Kayanne, H., Iijima, H., McClanahan, T.R., Behera, S.K., Yamagata, T., 2011. Footprints of IOD and ENSO in the Kenyan coral record. Geophys. Res. Lett. 38 http://dx.doi.org/10.1029/2011GL049877.
Nakamura, N., Kayanne, H., Iijima, H., McClanahan, T.R., Behera, S.K., Yamagata, T., 2009. Mode shift in the Indian Ocean climate under global warming stress. Geophys. Res. Lett. 36 http://dx.doi.org/10.1029/2009GL040590.
Nash, D.J., De Cort, G., Chase, B.M., Verschuren, D., Nicholson, S.E., Shanahan, T.M., Asrat, A., Lézine, A.-M., Grab, S.W., 2016. African hydroclimatic variability during the last 2000 years. Quat. Sci. Rev. 154, 1–22. http://dx.doi.org/10.1016/j.quascirev.2016.10.012.
Nicholson, S.E., 2001. Climatic and environmental change in Africa during the last two centuries. Clim. Res. 17, 123–144. http://dx.doi.org/10.3354/cr017123.
Oppo, D.W., Rosenthal, Y., Linsley, B.K., 2009. 2,000-year-long temperature and hydrology reconstructions from the Indo-Pacific warm pool. Nature 460, 1113–1116. http://dx.doi.org/10.1038/nature08233.
PAGES 2k Consortium, 2013. Continental-scale temperature variability during the past two millennia. Nat. Geosci. 6, 339–346. http://dx.doi.org/10.1038/ngeo1849.
Partin, J.W., Cobb, K.M., Adkins, J.F., Clark, B., Fernandez, D.P., 2007. Millennial-scale trends in west Pacific warm pool hydrology since the last glacial maximum. Nature 449, 452–455. http://dx.doi.org/10.1038/nature06164.
Partin, J.W., Quinn, T.M., Shen, C.C., Okumura, Y., Cardenas, M.B., Siringan, F.P., Banner, J.L., Lin, K., Hu, H.M., Taylor, F.W., 2015. Gradual onset and recovery of the Younger Dryas abrupt climate event in the tropics. Nat. Commun. 6 http://dx.doi.org/10.1038/ncomms9061.
Perrin, C., Prestimonaco, L., Servelle, G., Tilhac, R., Maury, M., Cabrol, P., 2014. Aragonite–calcite speleothems: identifying original and diagenetic features. J. Sediment. Res. 84, 245–269.
Risi, C., Bony, S., Vimeux, F., 2008. Influence of convective processes on the isotopic composition (δ18O and δD) of precipitation and water vapor in the tropics: 2. Physical interpretation of the amount effect. J. Geophys. Res. 113, D19306. http://dx.doi.org/10.1029/2008JD009943.
Rozanski, K., Araguás-Araguás, L., Gonfiantini, R., 1993. Isotopic patterns in modern global precipitation. Geophys. Monogr. Ser. 78, 1–36.
Ruggieri, E., 2013. A Bayesian approach to detecting change points in climatic records. Int. J. Climatol. 33, 520–528. http://dx.doi.org/10.1002/joc.3447.
Russell, J.M., Johnson, T.C., 2007. Little ice age drought in equatorial Africa: intertropical convergence zone migrations and El Niño–southern oscillation variability. Geology 35, 21–24. http://dx.doi.org/10.1130/G23125A.1.
Sachs, J.P., Sachse, D., Smittenberg, R.H., Zhang, Z., Battisti, D.S., Golubic, S., 2009. Southward movement of the Pacific intertropical convergence zone AD 1400–1850. Nat. Geosci. 2, 519–525. http://dx.doi.org/10.1038/ngeo554.
Saji, N.H., Goswami, B.N., Vinayachandran, P.N., Yamagata, T., 1999. A dipole mode in the tropical Indian Ocean. Nature 401, 360–363. http://dx.doi.org/10.1038/43854.
Schneider, T., Bischoff, T., Haug, G.H., 2014. Migrations and dynamics of the intertropical convergence zone. Nature 513, 45–53. http://dx.doi.org/10.1038/nature13636.
Schott, F.A., McCreary Jr., J.P., 2001. The monsoon circulation of the Indian Ocean. Prog. Oceanogr. 51, 1–123. http://dx.doi.org/10.1016/S0079-6611(01)00083-0.
Stein, A.F., Draxler, R.R., Rolph, G.D., Stunder, B.J.B., Cohen, M.D., Ngan, F., 2015. NOAA's HYSPLIT atmospheric transport and dispersion modeling system. Am. Meteorol. Soc. 96, 2059–2077. http://dx.doi.org/10.1175/bams-d-14-00110.1.
Tarutani, T., Clayton, R.N., Mayeda, T.K., 1969. The effect of polymorphism and magnesium substitution on oxygen isotope fractionation between calcium carbonate and water. Geochim. Cosmochim. Acta 33, 987–996. http://dx.doi.org/10.1016/0016-7037(69)90108-2.
Tierney, J.E., Russell, J.M., Sinninghe Damsté, J.S., Huang, Y., Verschuren, D., 2011. Late Quaternary behavior of the East African monsoon and the importance of the Congo air boundary. Quat. Sci. Rev. 30, 798–807. http://dx.doi.org/10.1016/j.quascirev.2011.01.017.
Tierney, J.E., Smerdon, J.E., Anchukaitis, K.J., Seager, R., 2013. Multidecadal variability in East African hydroclimate controlled by the Indian Ocean. Nature 493, 389–392. http://dx.doi.org/10.1038/nature11785.
Tierney, J.E., Ummenhofer, C.C., deMenocal, P.B., 2015. Past and future rainfall in the Horn of Africa. Sci. Adv. 1, e1500682. http://dx.doi.org/10.1126/sciadv.1500682.
Tozuka, T., Luo, J.-J., Masson, S., Yamagata, T., 2007. Decadal modulations of the Indian Ocean dipole in the SINTEX-F1 coupled GCM. J. Clim. 20, 2881–2894. http://dx.doi.org/10.1175/jcli4168.1.
Ummenhofer, C.C., England, M.H., Reason, C.J.C., Gupta, Sen, A., England, M.H., Reason, C.J.C., 2009. Contributions of Indian Ocean sea surface temperatures to enhanced East African rainfall. Am. Meteorol. Soc. 22, 993–1013. http://dx.doi.org/10.1175/2008JCLI2493.1.
UNICEF, 2012. 2012 Africa Snapshot. http://www.unicef.org/madagascar/eng/wes_15164.html (accessed 7.28.16).
Vellinga, M., Wood, R.A., 2002. Global climatic impacts of a collapse of the atlantic thermohaline circulation. Clim. Change 54, 251–267. http://dx.doi.org/10.1023/A:1016168827653.
Verschuren, D., Damsté, J.S.S., Moernaut, J., Kristen, I., Blaauw, M., Fagot, M., Haug, G.H., van Geel, B., De Batist, M., Barker, P., Vuille, M., Conley, D.J., Olago, D.O., Milne, I., Plessen, B., Eggermont, H., Wolff, C., Hurrell, E., Ossebaar, J., Lyaruu, A., van der Plicht, J., Cumming, B.F., Brauer, A., Rucina, S.M., Russell, J.M., Keppens, E., Hus, J., Bradley, R.S., Leng, M., Mingram, J., Nowaczyk, N.R., 2009. Half-precessional dynamics of monsoon rainfall near the East African equator. Nature 462, 637–641. http://dx.doi.org/10.1038/nature08520.
Verschuren, D., Laird, K.R., Cumming, B.F., 2000. Rainfall and drought in equatorial east Africa during the past 1,100 years. Nature 403, 410–414. http://dx.doi.org/10.1038/35000179.
Voarintsoa, N.R.G., Wang, L., Railsback, L.B., Brook, G.A., Liang, F., Cheng, H., Edwards, R.L., 2017. Multiple proxy analyses of a U/Th-dated stalagmite to reconstruct paleoenvironmental changes in northwestern Madagascar between 370CE and 1300CE. Palaeogeogr. Palaeoclimatol. Palaeoecol. 469, 138–155. http://dx.doi.org/10.1016/j.palaeo.2017.01.003.
Vuille, M., Burns, S.J., Taylor, B.L., Cruz Jr., F.W., Bird, B.W., Abbott, M.B., Kanner, L.C., Cheng, H., Novello, V.F., 2012. A review of the South American monsoon history as recorded in stable isotopic proxies over the past two millennia. Clim. Past 8, 1309–1321. http://dx.doi.org/10.5194/cp-8-1309-2012.
Wang, X., Auler, A.S., Edwards, R.L., Cheng, H., Cristalli, P.S., Smart, P.L., Richards, D.A., Shen, C.C., 2004. Wet periods in northeastern Brazil over the past 210 kyr linked to distant climate anomalies. Nature 432, 740–743. http://dx.doi.org/10.1038/nature03067.
Wang, X., Auler, A.S., Edwards, R.L., Cheng, H., Ito, E., Solheid, M., 2006. Interhemispheric anti-phasing of rainfall during the last glacial period. Quat. Sci. Rev. 25, 3391–3403. http://dx.doi.org/10.1016/j.quascirev.2006.02.009.
Wang, X., Auler, A.S., Edwards, R.L., Cheng, H., Ito, E., Wang, Y., Kong, X., Solheid, M., 2007. Millennial-scale precipitation changes in southern Brazil over the past 90,000 years. Geophys. Res. Lett. 34 http://dx.doi.org/10.1029/2007GL031149.
Wang, Y., Cheng, H., Edwards, R.L., Kong, X., Shao, X., Chen, S., Wu, J., Jiang, X., Wang, X., An, Z., 2008. Millennial- and orbital-scale changes in the East Asian monsoon over the past 224,000 years. Nature 451, 1090–1093. http://dx.doi.org/10.1038/nature06692.
Wassenburg, J.A., Scholz, D., Jochum, K.P., Cheng, H., Oster, J., Immenhauser, A., Richter, D.K., Häger, T., Jamieson, R.A., Baldini, J.U.L., Hoffmann, D.,

Breitenbach, S.F.M., 2016. Determination of aragonite trace element distribution coefficients from speleothem calcite–aragonite transitions. Geochim. Cosmochim. Acta 190, 347–367. http://dx.doi.org/10.1016/j.gca.2016.06.036.
Webster, P.J., Moore, A.M., Loschnigg, J.P., Leben, R.R., 1999. Coupled ocean–atmosphere dynamics in the Indian Ocean during 1997–98. Nature 401, 356–360. http://dx.doi.org/10.1038/43848.
World Bank, 2015. World Development Indicators. http://databank.worldbank.org/data/reports.aspx?source=2&country=MDG# (accessed 7.28.16).
Yan, H., Wei, W., Soon, W., An, Z., Zhou, W., Liu, Z., 2015. Dynamics of the intertropical convergence zone over the western Pacific during the little ice age. Nat. Geosci. 8, 315–320. http://dx.doi.org/10.1038/ngeo2375.
Zhang, R., Delworth, T.L., 2005. Simulated tropical response to a substantial weakening of the Atlantic thermohaline circulation. J. Clim. 18, 1853–1860. http://dx.doi.org/10.1175/jcli3460.1.
Zinke, J., Pfeiffer, M., Timm, O., Dullo, W.C., Brummer, G.J.A., 2009. Western Indian Ocean marine and terrestrial records of climate variability: a review and new concepts on land–ocean interactions since AD 1660. Int. J. Earth Sci. Geol. Rundsch. 98, 115. http://dx.doi.org/10.1007/s00531-008-0365-5.